

AIRBORNE RADIOMETRIC MEASUREMENTS OF SEA SURFACE TEMPERATURE

Numerous survey flights have been made over areas of the North Atlantic to study the sea surface radiometric properties at infrared wavelengths. This article discusses the unique imaging radiometer used, and how the data obtained illustrate the effects of such factors as incidence angle, the atmosphere, and cloud reflections from the sea surface on estimates of surface temperature.

INTRODUCTION

Sea surface temperature is one of the most important and extensively measured properties of the marine environment. Weather patterns and climate changes are known to be significantly influenced by long-term variations in sea surface temperature. Major water masses and current systems in the world's oceans can be readily identified by differences in surface temperature, as can oceanic fronts formed in the confluence zone of two or more currents. Large meanders of such ocean boundary currents as the Gulf Stream frequently break off and form mesoscale eddies that, because of prominent surface temperature signatures, can be tracked for several months as the eddy migrates over large distances. In coastal regions, horizontal variations in surface temperature are often associated with upwelling events, a finding exploited by the fishing industry to locate areas of biological activity.

Several techniques are used to monitor sea surface temperature. Oceanographers have traditionally used the so-called "bucket method" whereby near-surface water is sampled and its temperature measured with a thermometer. Slightly deeper water temperatures are measured with sensors mounted in the cooling-water intake ports on surface ships. Synoptic observations are nearly impossible with *in situ* techniques, however. In 1953, Stommel *et al.*¹ were the first investigators to use an airborne infrared radiation thermometer to track the northern edge of the Gulf Stream. The advent, in the 1960's, of meteorological satellites with scanning infrared radiometers provided the first opportunity to observe large ocean areas where upwelling and boundary currents produced large enough horizontal temperature gradients to be detectable above atmospheric and measurement noise. Since then, radiometer sensitivities have increased, and it is now possible to infer sea surface temperature averaged over an area of about 1 square

kilometer to an accuracy of about 1°C from space platform data. Such data, when combined with measurements from aircraft and ship surveys, are extremely valuable for understanding ocean-atmosphere energy exchange processes.

This article describes results from numerous surveys conducted by APL over regions of the North Atlantic since 1977 to study sea surface temperature variations by means of an ultrasensitive airborne infrared radiometer. This instrument, fabricated by Bendix Aerospace Systems Operations under APL subcontract, is specially designed for oceanographic measurements and has provided us with a unique capability for precision radiometric measurements.

SEA SURFACE RADIOMETRY

The application of infrared radiometry to remote measurements of sea surface temperature is based on the fact that water is a strong absorber of electromagnetic energy at 2 to 13 micrometers (μm), the infrared wavelengths of interest. Consequently, it emits infrared energy approximately as an ideal blackbody at the sea surface temperature. The optical properties of the sea surface are then characterized by its surface emissivity $\epsilon(\theta)$ and reflectivity $r(\theta)$, where Kirchoff's law requires the relationship $r(\theta) = 1 - \epsilon(\theta)$. The surface emissivity and reflectivity depend upon the incidence or nadir angle θ . To a first approximation, the sea surface can be considered to be flat. However, in some cases the effects of surface waves must be taken into account. Then the surface can be treated as a collection of facets, each small enough to be considered a flat surface with a specified slope. Since infrared wavelengths are very small compared to the wavelengths of surface waves, the principles of geometric optics can be applied to each facet, and diffraction effects can be ignored. An effective emissivity or reflectivity that is dependent upon the distribution of wave slopes can then be calculated. Typi-

cally, if the average root-mean-square wave slope is 10° , the reflectivity is only about 5% higher than the reflectivity of a smooth surface for an incidence angle of 45° .

Infrared wavelengths useful for remote sensing are those for which atmospheric absorption is small. The best windows are found in the wavelength intervals 3.6 to 4.0 μm and 10 to 12 μm . At 10.6 μm , the emissivity and reflectivity of water are 0.992 and 0.008, respectively, at normal incidence.

If atmospheric effects are ignored, the sea surface radiance, $N(T_R)$, can be expressed as the sum of emitted and reflected contributions,

$$N(T_R(\theta)) = \epsilon(\theta)N_B(T_0) + r(\theta)N_S(\theta), \quad (1)$$

where $N_B(T_0)$ is the Planck function evaluated at the surface temperature, T_0 , and integrated over the infrared wavelength band of interest, and $N_S(\theta)$ is the sky radiance at sea level in the same wavelength band.

The output of an infrared sensor is proportional to the radiance of the scene being viewed. By equating the measured radiance to that of an ideal blackbody, a value for the radiometric temperature, $T_R(\theta)$, can be obtained by inverting the Planck function. In general, this value will differ from T_0 because of the reflected sky radiance contribution. This difference is typically a few tenths of a degree.

In most situations, the atmosphere between the radiometer and the sea surface cannot be neglected. This intervening atmosphere attenuates the energy coming from the sea surface while at the same time it emits additional infrared energy into the radiometer. The previous expression for the total radiance then becomes

$$N(T_R(\theta)) = \mathfrak{J}_A(\theta)\epsilon(\theta)N_B(T_0) + \mathfrak{J}_A(\theta)r(\theta)N_S(\theta) + N_A(\theta), \quad (2)$$

where $\mathfrak{J}_A(\theta)$ represents the atmospheric transmission and $N_A(\theta)$ represents the emissions in the intervening atmosphere. $\mathfrak{J}_A(\theta)$ and $N_A(\theta)$ are related to each other and are dependent upon the vertical temperature profile and the constituents in the atmosphere. The measured radiometric temperature is generally lower than the true surface temperature because the intervening atmosphere is usually cooler than the water surface. For infrared wavelengths in the 10 to 12 μm band, this difference is about 1°C for an airborne radiometer at an altitude of 1 kilometer and about 3 to 6°C for a satellite radiometer.

Accurate determination of sea surface temperature from radiometric measurements requires knowledge

of the radiative transfer processes in the earth's atmosphere in order to estimate the correction to be applied to the radiometric temperature. Uncertainties in making this correction currently limit satellite-derived surface temperatures to accuracies on the order of 1°C . With aircraft measurements, the accuracy can be improved by an order of magnitude if the atmospheric effects are measured at several altitudes and appropriately combined with the surface radiance data.

The precise meaning of T_0 as expressed in Eq. 2 needs to be understood when comparing surface temperatures obtained remotely with those from *in situ* observations. At the air-sea interface, there is generally a loss of energy from the sea surface to the atmosphere. Because this transfer takes place by molecular processes at the interface, a thermal boundary layer or "cool skin" develops in the upper 0.1 to 1.0 millimeter of the water, within which the temperature increases linearly with depth. This temperature gradient is proportional to the net heat lost to the atmosphere and is typically in the range of 2 to 5°C per centimeter.

The optical attenuation lengths for water at infrared wavelengths are less than the thickness of this cool skin at the surface. When the linear temperature gradient near the surface is taken into account, it can be shown that T_0 in Eq. 2 is identical to the temperature within the cool skin at the depth equal to the optical attenuation length for the wavelength of the infrared energy being measured.² Thus, T_0 will be typically 0.01 to 0.05°C warmer than the temperature right at the air-sea interface. Nevertheless, it is a more accurate measure of the interface temperature than are temperatures obtained with *in situ* techniques. The latter really provide bulk water temperature rather than surface temperature, a difference that can often be as large as several tenths of a degree.

RADIOMETER SYSTEM

The radiometer used for the surveys described in this article is a two-channel instrument that measures infrared energy in the spectral bands of 3.6 to 4.1 μm and 10.1 to 11.1 μm . The system, consisting of an optics unit housed in an aerodynamic pod and a control console, is flown on an RP-3A aircraft operated by the U.S. Naval Oceanographic Office. Attached to the front of the optics unit is a scan mirror that rotates about an axis parallel to the flight direction, thereby causing the instantaneous field of view (IFOV) to traverse the sea surface and overhead sky in a raster-like fashion as the aircraft advances. To avoid the aircraft's reflection on the sea surface, the axis of the IFOV projects 20° forward; therefore, the IFOV sweeps out a cone of 70° half-angle as the scan

mirror executes a complete revolution. The total field of view consists of two 105° arc segments oriented with respect to the nadir and zenith (Fig. 1). In one revolution of the scan mirror, the IFOV scans the ocean from -60° to +45° relative to the nadir, the sky from +45° to -60° relative to the zenith, and a field-filling external blackbody. Operation and data acquisition are controlled by a PDP-11R/20 minicomputer that electronically processes the detector signals into a digital format and presents them for recording on a magnetic tape unit and for display as real-time imagery on a TV monitor. Figure 2 is a block diagram of the radiometer.

The aerodynamic housing containing the optics unit is mounted above the aircraft radome (Fig. 3). The pod is 20 inches in diameter and approximately 9 feet in length. The nose section has 7-inch-wide openings extending around the pod circumference to permit unobstructed viewing of the desired angular range of sea surface and overhead sky. Two porous-screen fences and a solid deflector are placed forward of the viewing ports to control the boundary layer air flow over the openings.

The optical layout of the radiometer is shown in Fig. 4. The radiant energy reflected by the scan mirror passes through an antireflection-coated zinc

selenide window into the liquid-nitrogen-cooled optics and detector assembly. Both the reflecting surface of the scan mirror and the entrance window are temperature controlled so that their contribution to the detected radiance is constant. A germanium objective lens images the scene onto two iris diaphragms, using a dichroic beam splitter to separate the beams. The beam transmitted by the beam splitter is bandpass limited to 10.1 to 11.1 μm and is concentrated by a germanium field lens located behind the iris onto a lead-tin-telluride detector. The energy reflected by the beam splitter uses a similar system, but the detector is indium-antimonide, and a separate bandpass filter limits the spectral band to 3.6 to 4.1 μm. The variable aperture iris mounted in the focal plane of the objective lens in front of each detector permits operator selection of the IFOV over the range from 0.01 to 0.1 radian. This range can be changed to 0.02 to 0.2 radian by changing the objective lens. With each lens at the maximum aperture,

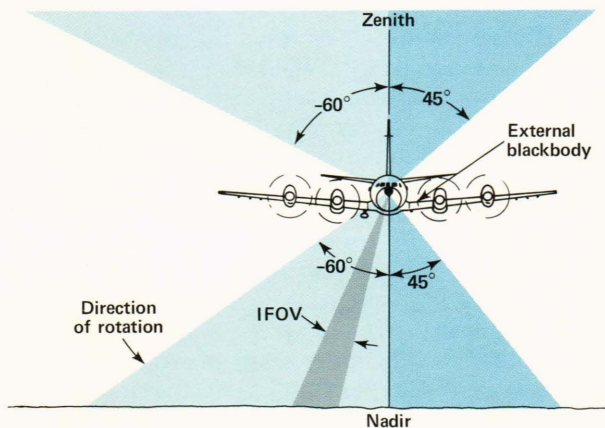


Figure 1 — Radiometer scan geometry. In one revolution of the scan mirror, the IFOV scans the ocean from -60° to +45° of the nadir, the sky from +45° to -60° of the zenith, and a field-filling external blackbody.



Figure 3 — Radiometer installation on RP-3A aircraft. The optics unit of the radiometer is mounted in a pod located above the radome of the aircraft. The forward extension and airstream control surfaces minimize air velocities within the pod.

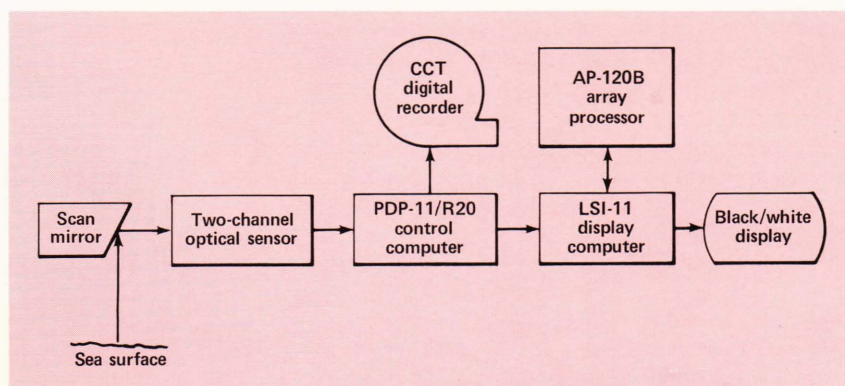


Figure 2 — Radiometer block diagram. The surface radiance is measured by a two-channel optical sensor under the control of a computer. The output is digitized and recorded and is available for real-time black/white display.

the instrument has a noise equivalent temperature difference (NE Δ T) of 0.002 to 0.003°C in each spectral band.

Calibration and reference signals are obtained from two temperature-controlled blackbodies. The external blackbody is used to calibrate the system and to provide a reference source matching the scene radiance. The internal blackbody, viewed by reflection from a chopper blade, is used to eliminate electronics drift. When the radiometer is being calibrated, the scan mirror is fixed to view the external blackbody continuously. The rotating chopper blades alternately expose the external and internal blackbodies 75 times per second. Calibration factors are determined by recording detector outputs at several external blackbody temperatures and computing a linear least-squares fit of detector output to both external blackbody temperature and radiance. It is desirable to calibrate and operate the radiometer using

reference temperatures near the anticipated scene temperature, which can then be determined by comparing the detector output from the blackbody with that from the scene.

An electronics compartment mounted at the rear of the dewar assembly contains a preamplifier, a gain-programmable amplifier, a dumped integrator, a sample-and-hold module, and a 15-bit analog-to-digital converter for each detector. Each detector is sampled 75 times per second in the calibration mode and 225 times per second in the scanning mode.

The entire optics unit is mounted on gimbals to compensate for aircraft pitch motion. The scan mirror rotation is adjusted to compensate for roll motion. This two-axis compensation is derived from a vertical gyro attached to the optics unit.

Figure 5 shows the control console and display unit. The PDP-11R/20 computer with 20K memory is interfaced to the operator control panel and the op-

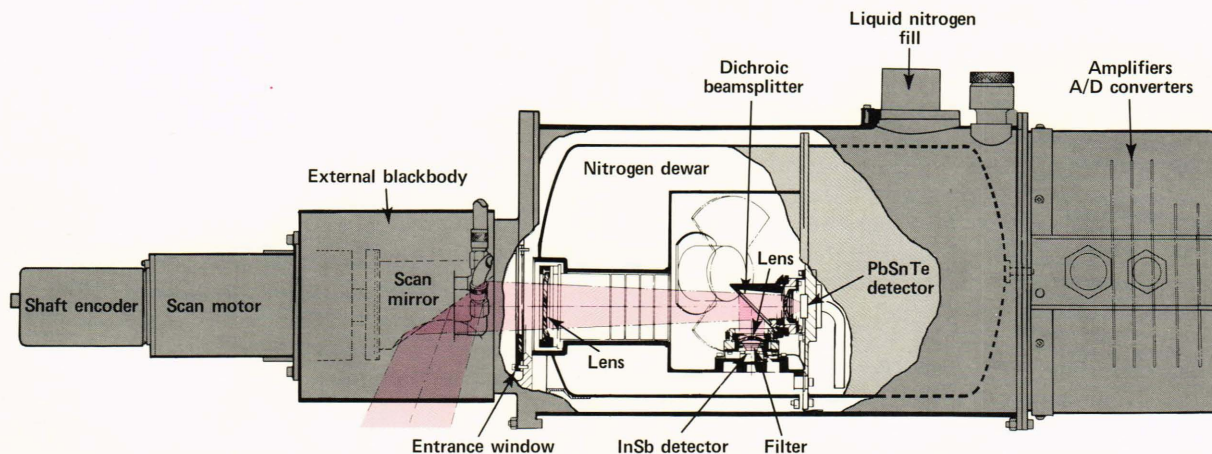


Figure 4 — Optics unit. The optics unit includes a scan mirror system and a liquid-nitrogen-cooled optical assembly. The external scene is imaged by an objective lens onto the detector assembly where filters isolate the two spectral bands and detectors measure the radiation. Amplifiers and analog-to-digital converters are mounted close to the detectors.

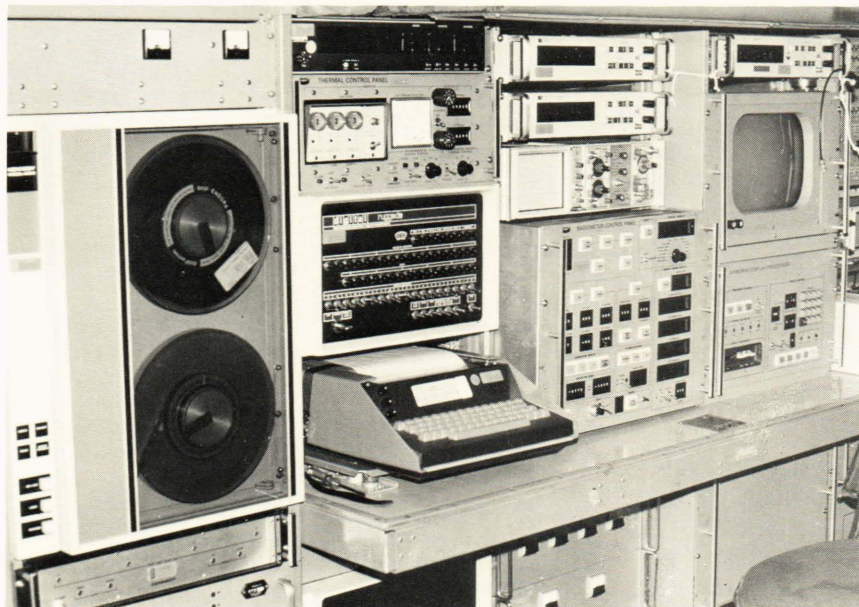


Figure 5 — Radiometer control console.

tics unit for system control and data acquisition. Numerical displays are provided for examining various system operating parameters. A Kennedy Model 9000 magnetic tape unit records the data. A display system provides the operator with a real-time moving window image on a TV monitor after removing apparent temperature variations caused by the dependence of the surface emissivity on incidence angle and enhancing small temperature differences from the nominal ocean surface temperature.

The ocean measurements are obtained with the system in the scan mode, with the scan mirror rotating continuously at the rate chosen by the operator. The internal chopper is clear of the beam so that the detectors continuously view the external scene. One or two scans may be interrupted at periodic intervals to insert reference data. This is done by moving the chopper blade a quarter turn so that the detectors see the internal blackbody. The external blackbody is sampled once per scan mirror revolution. The IFOV and rotation rate of the scan mirror are adjustable by the operator to control both the along-track and cross-track coverage.

During radiometer surveys, ancillary data are recorded from atmospheric, oceanographic, and avionics sensors on board the aircraft. Air temperature, dewpoint, pressure, winds, altitude, speed, position, and aircraft attitude are continuously recorded, along with nadir and zenith radiance (8 to 13 μm). A laser wave-height profiler is used to monitor sea conditions, and air-launched expendable bathythermographs (AXBT) measure temperature profiles in the water column. These data are recorded by the Birdseye Airborne Survey System (BASS), a computer-controlled data acquisition system designed and fabricated by the APL Space Department for the U.S. Naval Oceanographic Office.³

SURVEY RESULTS

Nineteen survey flights over various areas of the North Atlantic were made between 1977 and 1979 to study sea surface temperature variations. A typical flight included several hours of data collection at a nominal aircraft velocity of 200 knots. Altitudes between 500 and 3000 feet were generally used to minimize atmospheric degradations. Data from these surveys have been processed to illustrate how factors such as incidence angle, atmospheric effects, and cloud reflections from the sea surface affect estimates of surface temperature obtained from infrared radiometers. Some general characteristics of the sea surface radiance at infrared wavelengths have also been distilled from measurements made during these surveys.

Incidence Angle Effects

The reflectivity of the sea surface, and consequently its emissivity, varies with wavelength and incidence or nadir angle. This variation can be computed from the Fresnel relations and the optical constants of water. When an infrared radiometer views the sea

surface at increasing incidence angles, the emitted energy contribution to the total radiance will decrease and the reflected sky radiance contribution will increase. Because the sky radiance is normally less than that of the sea, a net decrease in total radiance is measured with increasing incidence angle.

The magnitude of this angular variation was determined through use of several data sets from different flights. Clear sky conditions with minimal horizontal surface temperature changes were chosen to avoid spurious contributions. Figure 6 is an example of the variation of radiometric temperature with nadir angle measured at an altitude of 750 feet during one of those flights. The ordinate is the difference in radiometric temperature between the value at the minimum nadir angle of 20° and the value at the nadir angle θ . By averaging each data point over 48 consecutive scans, deviations from the best-fit curve are generally reduced to less than 0.01°C. Note that both the difference and the rate of change of the difference increase with nadir angle. At nadir angles less than 45°, the difference is less than 0.1°C. The ability to measure such changes precisely has yielded a valuable body of data for comparison with models of sea surface reflectivity that attempt to account for sea surface roughness and atmospheric effects.⁴

Atmospheric Effects

To define the atmospheric effects, atmospheric profiles are measured during each survey by flying for one minute at each of several altitudes from 500 to 3000 feet, the choice depending on the cloud height. Figure 7a shows the radiometric surface temperature at the minimum nadir angle (20°) measured as a function of altitude on October 2, 1979. The decrease with increasing altitude is approximately 0.5°C per 1000 feet. Extrapolation of such data to zero altitude can often be in error by a few tenths of a degree because of surface temperature changes and atmospheric variations over the region surveyed. More extensive computations using measurements in both infrared bands and the sky radiance data at each

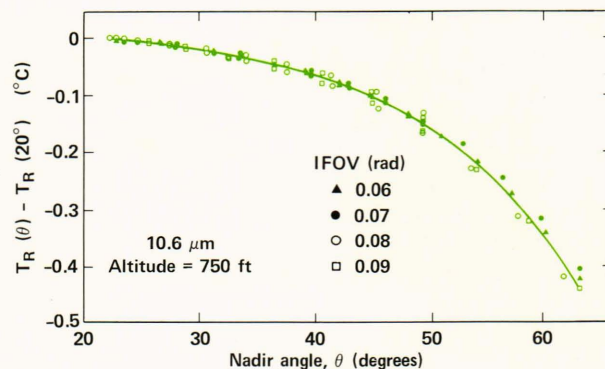


Figure 6 — Radiometric temperature variation with nadir angle. As the nadir angle increases, the changing surface emissivity and reflectivity cause a net decrease in the radiometric temperature of the ocean.

altitude can be made to minimize the uncertainty in the extrapolated temperature.

The radiometric temperature variation with nadir angle for several altitudes is shown in Fig. 7b. Each curve is referenced to a zero temperature difference

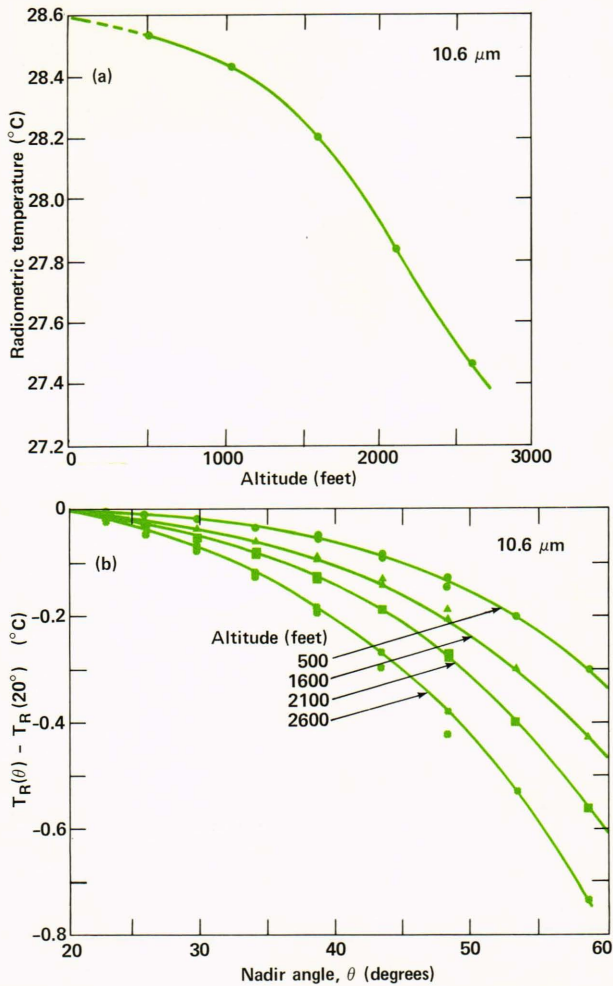


Figure 7 — Radiometric temperature change with altitude. The surface radiometric temperature decreases as the atmospheric thickness increases with altitude (a) and with nadir angle (b).

at 20° nadir angle. The difference between curves is a relative measure of the contribution from the additional amount of intervening atmosphere.

Cloud Reflections

Clouds above the sea surface can be thought of as localized radiators of infrared energy with a temperature corresponding to that of the atmosphere at the height of the clouds. A small amount of this energy will be reflected by the sea surface, and a radiometer will record an image of the cloud blurred by the surface waves in the same manner that the waves blur the sun's image to produce the familiar sun-glitter pattern.

Images of this phenomenon have been recreated from our radiometer measurements by applying a series of algorithms that generate gray-level imagery. These algorithms resample each scan to produce an equally spaced array of samples on the surface, filter the data in two dimensions to remove the nadir angle variation discussed above, normalize by the local variance, interpolate to the correct geometry, and then assign gray levels to enhance and display the features of interest appropriately. Representative thermal images of the sea surface and overhead sky showing scattered clouds and their reflections along a 6-nautical-mile track are shown in Fig. 8. These images were produced from data recorded as the aircraft flew from left to right along a line marked by the 0° scan angle while scanning from -60 to +45° transverse to the flight direction. Light tones represent areas with warmer radiometric temperatures than adjacent dark areas. The light areas in the sea-surface thermal image are cloud reflections caused by the presence of the scattered clouds above the aircraft and clearly seen in the thermal image of the overhead sky. The curve at the bottom of Fig. 8 is a trace through the sea surface image at the -45° scan angle position. It can be seen that the cloud reflections contribute distinct changes in radiometric temperature of 0.15 to 0.30°C over characteristic distances of about a nautical mile resulting from the blurring of the surface waves. The upward-scanning capability of our radiometer allows one to monitor and record the cloud

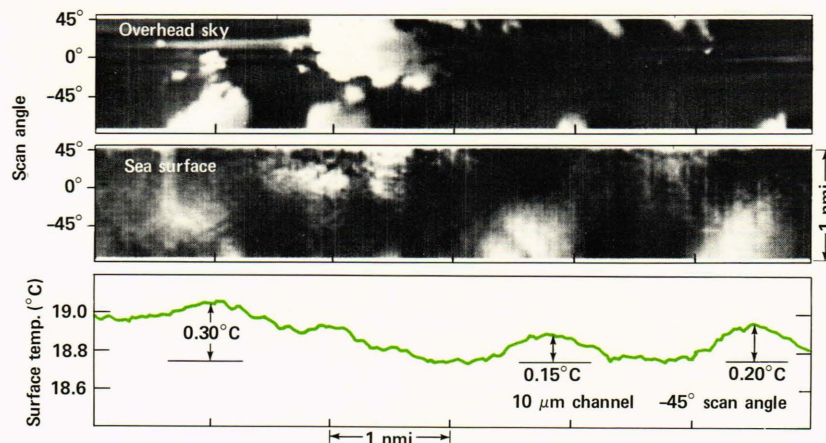


Figure 8 — Reflected cloud image. Clouds are visible by direct observation of the overhead sky and by reflection from the ocean surface. The trace in the bottom figure shows the variation recorded along the -45° scan angle line through the sea surface temperature image.

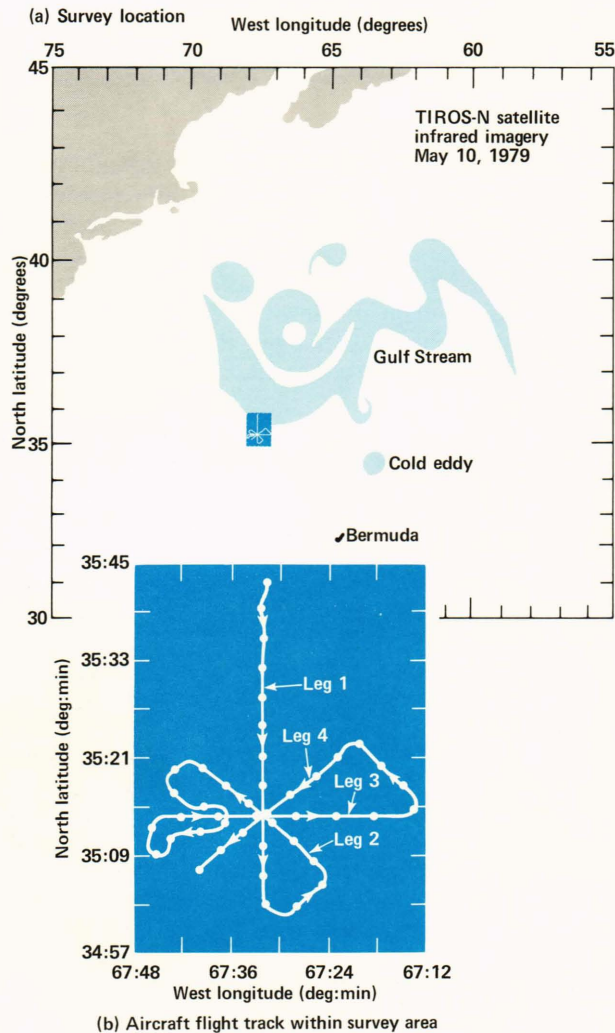


Figure 9 — Survey location and flight track. On May 11, 1979, the rosette flight track of (b) was flown across the southern edge of the Gulf Stream identified in the Tiros-N satellite infrared imagery sketched in (a).

conditions that exist during each survey and often to discriminate apparent from true surface temperature variations.

General Radiance Characteristics

One of the objectives in conducting these surveys is to be able to describe better how the surface radiance properties depend on the ocean environment. A variety of oceanographic and Navy related problems can then be addressed using radiometric models refined and validated by such measurements. Research in this area is still continuing, but some general features of the surface radiance have emerged from analyses completed to date.

Some of the elements of this work can be illustrated by considering a survey flown on May 11, 1979, in the Sargasso Sea. The location of the survey and the flight track flown, consisting of four intersecting legs at different compass headings, are shown in Fig. 9. Tiros-N satellite imagery acquired on May

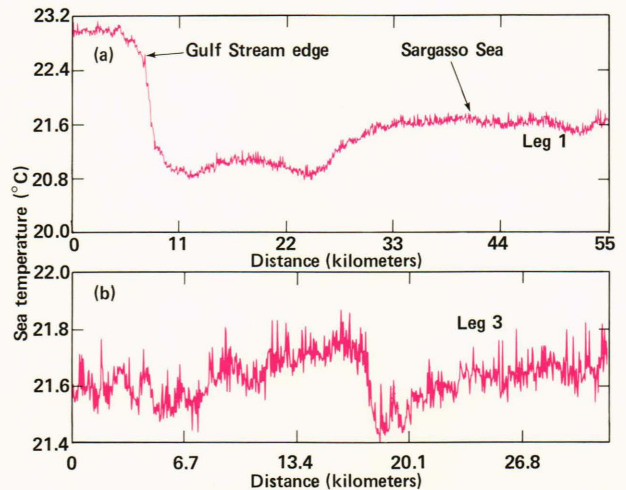


Figure 10 — Surface temperature: Leg 1 (a) and Leg 3 (b), May 11, 1979. The temperature variations along Legs 1 and 3 of the rosette in Fig. 9 show different magnitudes. In Leg 1, the Gulf Stream crossing causes a 2°C change while Leg 3, parallel to the Gulf Stream, has variations of only 0.3°C .

10 shows the location of the Gulf Stream relative to the survey area. Note that the southern edge of the Stream protrudes into the northern portion of the survey area. The nominal aircraft speed was 210 knots and the altitude was 2600 feet during this survey. Circles are drawn on the flight track at one-minute intervals.

The surface temperature measured along the aircraft track during part of Leg 1 is plotted in Fig. 10a. The southern edge of the Gulf Stream can be seen near the beginning of the plot where the temperature drops rapidly from about 22.6°C to about 20.8°C . A little farther in the leg the surface temperature rises to about 21.6°C . Such large variations in surface temperature are commonly observed near intersections of different water masses. In contrast, the surface temperature is generally more uniform within the Sargasso Sea, as shown by the surface temperature plot along Leg 3 (Fig. 10b). Here the temperatures are within $\pm 0.2^{\circ}\text{C}$ of the mean value of 21.6°C .

The difference in surface temperature variability between Legs 1 and 3 can be quantified by computing the probability distribution histogram for the fluctuations about the mean surface temperature in each leg. The results are shown in Figs. 11a and 11b for Legs 1 and 3, respectively. The smooth curve in each figure represents a Gaussian distribution with the same standard deviation as that of the data set plotted. For Leg 1, the standard deviation is 0.55°C ; the bimodal distribution results from the large temperature differences encountered during this leg. For Leg 3, the standard deviation is only 0.08°C , and the probability distribution histogram more closely approaches the Gaussian function. This nearly Gaussian distribution is frequently found to be a property of the radiometric temperature variations, especially when the variations occur over distances of a kilometer or less.

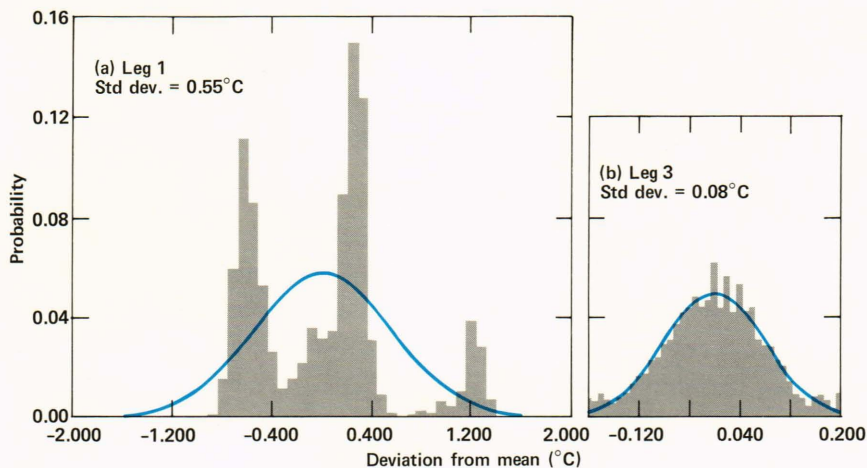


Figure 11 — Surface temperature histograms: Leg 1 (a) and Leg 3 (b), May 11, 1979. The temperature variations across the Gulf Stream (Leg 1) produce a large and bimodal probability distribution, whereas in the more uniform region (Leg 3), the probability distribution is close to the Gaussian profile indicated by the smooth curve.

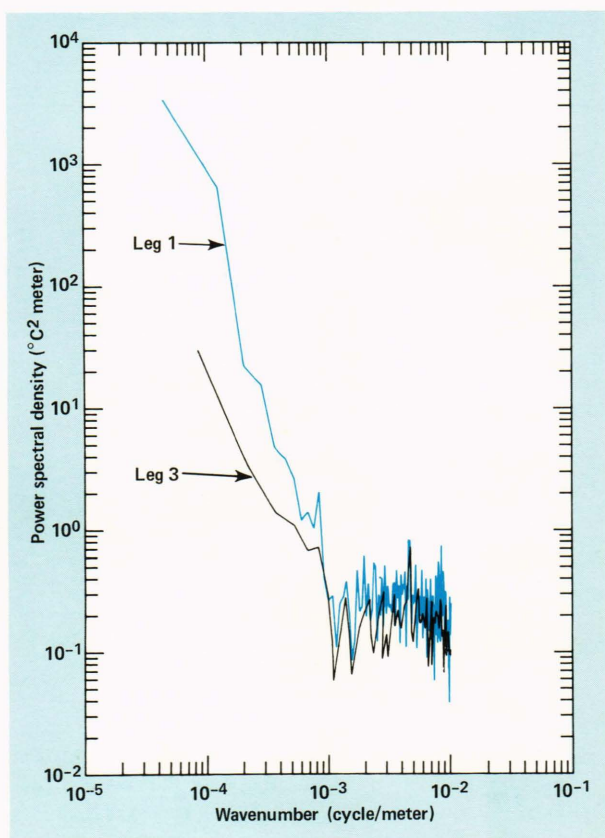


Figure 12 — Wavenumber variance spectra — Legs 1 and 3, May 11, 1979. The power spectral densities show that the temperature variations for Leg 1 are higher than those for Leg 3, primarily in the wavenumber range below 0.001 cycle per meter.

The length scales contributing to the radiance variations can be determined by computing the wavenumber variance spectrum. Spectra corresponding to

the traces in Fig. 10 are shown in Fig. 12. The spectrum for each leg exhibits a characteristic shape common to a variety of data wherein the variance decreases with increasing wavenumbers and then tends to level off at wavenumbers above 0.001 cycle per meter. When spectra obtained by flying different compass headings are compared, they generally show no significant differences at the high wavenumbers, implying that the short-wavelength surface temperature variations are fairly isotropic. However, the longer-wavelength variations associated with large-scale oceanic phenomena often exhibit considerable anisotropy.

CONCLUSION

The intent of this article has been to provide a brief overview of various aspects of remote sensing of sea surface temperature using infrared radiometers. The results presented are just a glimpse of the rich variety of sea surface temperature features that result from oceanic phenomena and air-sea interaction processes. At the very least, they provide adequate testimony to the role that precision instruments like the APL radiometer can play in the application of remote sensing techniques to oceanographic research.

REFERENCES

- ¹H. Stommel, W. S. von Arx, D. Parson, and W. S. Richardson, "Rapid Aerial Survey of Gulf Stream with Camera and Radiation Thermometer," *Science* **117**, 639-640 (1953).
- ²E. D. McAlister and W. McLeish, "Heat Transfer in the Top Millimeter of the Ocean," *J. Geophys. Res.* **74**, 3408-3414 (1969).
- ³C. E. Rehbein, "Birdseye Airborne Survey System, Volume 1, System Description," JHU/APL S3-E-019 (1976).
- ⁴K. Peacock, "Radiometric Temperature Characteristics of the Ocean Surface," JHU/APL STD-R-377 (1980).